

Micron-level Optimal Obstacle-avoidance Trajectory Planning for a Free-floating Space Robot with Predefined-time Convergence

Wen Yan¹ and Yicheng Liu¹

¹ College of Electric Engineering, Sichuan University, Chengdu 610065, China.

Correspondence should be addressed to Yicheng Liu; liuyicheng@scu.edu.cn

Abstract

With the development of human space exploration, the space environment is gradually filled with abandoned satellite debris and unknown micrometeorites, which will seriously affect capture motion of space robot. Hence, a novel fast collision-avoidance trajectory planning strategy for a dual-arm free-floating space robot (FFSR) with predefined-time pose feedback will be mainly studied to achieve micron-level tracking accuracy of end-effector in this paper. However, similar to control, the exponential feedback results in larger initial joint angular velocity relative to proportional feedback. Therefore, a GA-based optimization algorithm is used to reduce the control input, which is just the joint angular velocity. Firstly, a pose-error-based kinematic model of the FFSR will be derived from a control perspective. Then, a cumulative dangerous field (CDF) collision-avoidance algorithm is applied in predefined-time trajectory planning to achieve micron-level collision-avoidance trajectory tracking precision. In the end, a GA-based optimization algorithm is used to optimize the predefined-time parameter to obtain a motion trajectory of low joint angular velocity of robotic arms. The simulation results verify our conjecture and conclusion.

Introduction

The space exploration is an important human activity, and space satellites are often regarded as a necessary part of it [1-4]. However, many satellites are scrapped each year due to aging components or micrometeorite impacts, and these satellites are likely to cause secondary impacts on other normal satellites [5,6]. Hence, in order to reduce unnecessary losses, the satellite recovery has become an important task for space robots. At the same time, the robot obstacle avoidance algorithm is also needed to enable it to complete the task safely and not become the next fragment [7,8].

The dual-armed 6-DOF(degrees of freedom) robot is often mounted on the satellite base to perform capture missions because of its flexibility and versatility, and the space robot also floats freely to complete the capture mission. Hence, the dynamic coupling between the arm and the satellite base may lead to the pose deviation of the base, thus increasing the tracking error of the end-effector [9]. In order to keep pose of base stable, a motion planning strategy for the balance arm is adopted in the trajectory planning algorithm to offset dynamic coupling by some researchers. Agrawal and Shirumalla [10] proposed an iterative-search-based dual-arm motion planning method to stabilize the position of base, but attitude was not considered. Zhao et al. [11] presented a coordinated dynamics control scheme with zero internal forces to reduce the position and attitude error of base simultaneously. Based on that, Yan et al. [12]

studied the concept of base centroid virtual manipulator to reduce the pose error of base further. However, the above-mentioned methods cannot eliminate the errors of base and end-effector to zero theoretically. Moreover, when kinematic singularity occurs or the obstacle needs to be avoided, the error caused by additional algorithms will be further increased, and the previous method will be of little use. Fortunately, Liu et al. [13,14] presented a trajectory planning strategy with pose-feedback to eliminate the errors caused by singularity-avoidance and self-collision-avoidance method, but it cannot deal well with large cumulative error and the convergence time can also not be predicted.

Similar to control, because the essence of the feedback-based trajectory planning is to regard joint angular velocity of robotic arm as the control input and the velocity-level pose error obtained from the pose-error-based kinematic equation as the system output, the increase of joint angular velocity will be inevitable if exponential feedback is introduced to replace proportional feedback. Yoshio Yokose [15] applied genetic algorithm in the trajectory planning to obtain smooth joint angular velocity trajectory, but the tracking error is not considered primarily. Chen et al. [16] designed a considerate objective function of GA, but the tracking error will be large if there is a singular configuration in planned trajectory. Wu et al. [17] presented a GA-based singularity-free path planning for a space robot, and it can optimize the additional algorithm. However, none of the above methods can solve the problem of error elimination theoretically, and the error will inevitably increase if there are external interference, such as singularity and obstacle. Therefore, we try to solve the error problem theoretically by exponential feedback to obtain the high-precision motion trajectory of end-effector, and GA optimization strategy is only used to optimize the joint angular velocity trajectory to get the best trajectory planning strategy for the space robot.

Motivated the above issues, a GA-based optimal predefined-time trajectory planning for a FFSR is studied in this paper. The main purpose of this paper is to study how to obtain an optimal trajectory planning scheme for a space robot, which it is a continuing study. Therefore, the space robot model will adopt the more mature pose-error-based kinematic model that we studied earlier [13]. The main contributions of this paper lie in two aspects:

- 1) A novel GA-based predefined-time stability system method is studied to get the optimal parameter, which makes joint angular velocity smaller.
- 2) A predefined-time trajectory planning method for a FFSR system is proposed to stabilize the pose of base and achieve micron-level tracking precision in predefined time with dynamic coupling, singularity and obstacle.

In the following, Section 2 notes the related theoretic preliminaries. Section 3 introduces the pose-error-based kinematic model of a free-floating dual-arm space robotic system. Section 4 shows trajectory planning for the robotic system. Section 5 shows the simulation and analysis of the recent methods and the proposed method. Finally, section 6 presents the conclusion.

Preliminaries

Definition 1 [18]: Consider a system:

$$\dot{\mathbf{x}}(t) = \mathbf{f}(\mathbf{x}(t)), \mathbf{x}(0) = \mathbf{x}_0. \quad (1)$$

where the state variables of system are set to $\mathbf{x} = [x_1, x_2 \cdots x_n]^T \in \mathbb{R}^n$, $\mathbf{f}(\mathbf{x}): D \rightarrow \mathbb{R}^n$ is a continuous function, and $\mathbf{f}(0) = 0$. If the above system is finite-time stable and the minimum

upper bound of the settling time can be predicted to be T_c , the equilibrium in system (1) will be said to be predefined-time stable.

Lemma 1 [18]: Consider the following system:

$$\dot{\mathbf{x}} = -\frac{1}{mT_c} \exp(\|\mathbf{x}\|^m) \frac{\mathbf{x}}{\|\mathbf{x}\|} \quad (2)$$

where $0 < m < 1$, and T_c is a positive time parameter. The system in (2) is predefined-time stable and the convergence time maximum can be predefined as T_c by Definition 1.

Remark 1: A predefined-time function can be defined as:

$$\boldsymbol{\varphi}(\mathbf{x}; T_c, m) = \frac{1}{mT_c} \exp(\|\mathbf{x}\|^m) \frac{\mathbf{x}}{\|\mathbf{x}\|} \quad (3)$$

Pose Error Based Kinematic Modelling

As shown in Fig. 1, the proposed space robot mainly includes two 6-DOF PUMA560-type robotic arms, and they are mounted on the satellite base. Arm-1 is the mission arm and Arm-2 is the balance arm.

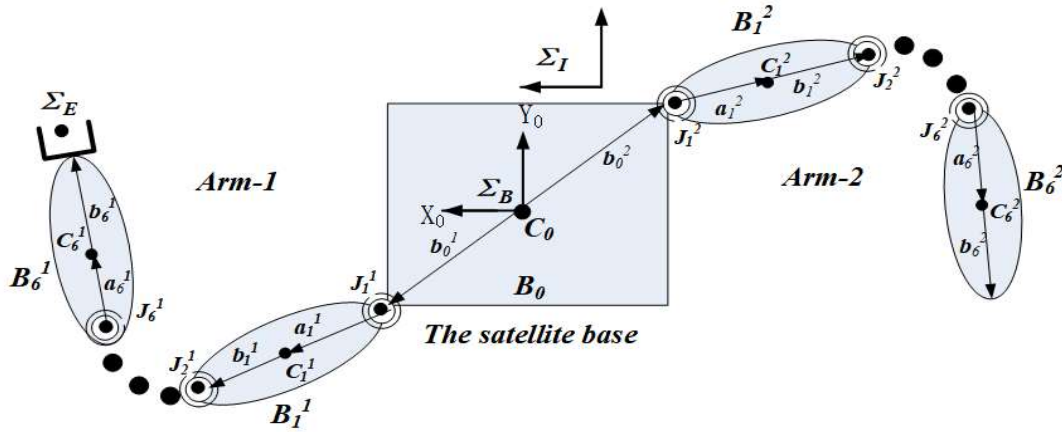


Figure 1. Model of a dual-arm FFSR system

According to “the pose error kinematic equation (17) and (18)” in our previous study [13], the pose-error kinematic relationship of end-effector and base can be expressed as (The cited velocity kinematic model can be referred to the Appendix, which is from [13]):

$$\dot{\mathbf{e}}_1 = \mathbf{J}_e \mathbf{V}_e - \mathbf{J}_{ed} \mathbf{V}_{ed} = \mathbf{J}_e (\mathbf{J}_0 \mathbf{V}_0 + \mathbf{J}_m^1 \dot{\boldsymbol{\Theta}}^1) - \mathbf{J}_{ed} \mathbf{V}_{ed}. \quad (4)$$

$$\dot{\mathbf{e}}_0 = \mathbf{J}_b \mathbf{V}_0 - \mathbf{J}_{bd} \mathbf{V}_{0d} = \mathbf{J}_b \mathbf{H}_0^{-1} (\mathbf{C} - \mathbf{J}_c^1 \dot{\boldsymbol{\Theta}}^1 - \mathbf{J}_c^2 \dot{\boldsymbol{\Theta}}^2) - \mathbf{J}_{bd} \mathbf{V}_{0d}. \quad (5)$$

where $\mathbf{e}_1 = [\mathbf{e}_e^T \ \boldsymbol{\sigma}_e^T]^T$, $\mathbf{e}_0 = [\mathbf{e}_b^T \ \boldsymbol{\sigma}_b^T]^T$, in which \mathbf{e} and $\boldsymbol{\sigma}$ denote the position and attitude error of FFSR, respectively; \mathbf{C} is the initial pose momentum of the system; \mathbf{J}_0 and \mathbf{J}_m^1 are the Jacobian matrixes of the base and Arm-1 of FFSR, respectively; \mathbf{J}_c^1 and \mathbf{J}_c^2 are the coupling inertia matrixes of Arm-1 and Arm-2, respectively; $\mathbf{V}_e = [\mathbf{v}_e^T \ \boldsymbol{\omega}_e^T]^T$ is the velocity vector of the end-effector; $\mathbf{V}_0 = [\mathbf{v}_0^T \ \boldsymbol{\omega}_0^T]^T$ is the velocity of base; $\mathbf{V}_{ed} = [\mathbf{v}_{ed}^T \ \boldsymbol{\omega}_{ed}^T]^T$ is the desired velocity of end-effector; \mathbf{V}_{0d} is the desired velocity of base which is set to 0 here; $\dot{\boldsymbol{\Theta}}^1 \in \mathbb{R}^{6 \times 1}$ and $\dot{\boldsymbol{\Theta}}^2 \in \mathbb{R}^{6 \times 1}$ are the joint angular velocity vector of Arm-1 and Arm-2 ($j=1,2$), respectively; \mathbf{H}_0 is the coupling inertia matrix of momentum conservation of FFSR. $\mathbf{J}_{e,b}$ and $\mathbf{J}_{ed,bd}$ are with (11),

$$\mathbf{J}_{e,b} = \begin{bmatrix} \mathbf{E}_3 & 0 \\ 0 & \frac{1}{4}G(\boldsymbol{\sigma}_{e,b}) \end{bmatrix}, \quad \mathbf{J}_{ed,bd} = \begin{bmatrix} \mathbf{E}_3 & 0 \\ 0 & \frac{1}{4}G(\boldsymbol{\sigma}_{ed,bd})\mathbf{R}_{ed,bd} \end{bmatrix}. \quad (6)$$

in which \mathbf{E}_3 is a 3 order identity matrix; $\mathbf{R}_{ed,bd} \in \mathbb{R}^{3 \times 3}$ is the rotational matrix which transforms the reference frame to the frame fixed on the end-effector or base, $G(\boldsymbol{\sigma}) = (1 - \boldsymbol{\sigma}^T \boldsymbol{\sigma})\mathbf{E}_3 + 2\tilde{\boldsymbol{\sigma}} + 2\boldsymbol{\sigma}\boldsymbol{\sigma}^T$.

Remark 2: The attitude error is in terms of Modified Rodrigues Parameter (MRP) [19], because the MRP can make attitude computation for robotic system small.

Trajectory Planning

Non-singular Trajectory Planning for a Dual-arm FFSR

Firstly, the joint angular velocity of robotic arm $\dot{\boldsymbol{\Theta}}$ can be seen as the control input, then we can control the velocity-level pose errors of the end-effector and base to converge in an expected convergence form by adjusting the joint angular velocity trajectory. Therefore, based on the proportional feedback in our previous study [13], the velocity-level pose errors equations (4) and (5) can be expressed as:

$$-k\mathbf{e}_1 = \dot{\mathbf{e}}_1 = \mathbf{J}_e \mathbf{V}_e - \mathbf{J}_{ed} \mathbf{V}_{ed} = \mathbf{J}_e (\mathbf{J}_0 \mathbf{V}_0 + \mathbf{J}_m^1 \dot{\boldsymbol{\Theta}}^1) - \mathbf{J}_{ed} \mathbf{V}_{ed}, \quad (7)$$

$$-k\mathbf{e}_0 = \dot{\mathbf{e}}_0 = \mathbf{J}_b \mathbf{V}_0 - \mathbf{J}_{bd} \mathbf{V}_{0d} = \mathbf{J}_b \mathbf{H}_0^{-1} (\mathbf{C} - \mathbf{J}_c^1 \dot{\boldsymbol{\Theta}}^1 - \mathbf{J}_c^2 \dot{\boldsymbol{\Theta}}^2) - \mathbf{J}_{bd} \mathbf{V}_{0d}. \quad (8)$$

where $k > 0$ is a proportional parameter.

However, the proportional convergence is often unable to cope with the timing tasks and large errors. Hence, a predefined-time stability system in Lemma 1 is applied in the time derivation of pose error of end-effector to obtain an exponential convergence, which can be expressed by Remark 1:

$$\dot{\mathbf{e}}_1 = -\boldsymbol{\varphi}(\mathbf{e}_1; T_c, m), \quad (9)$$

$$\dot{\mathbf{e}}_0 = -\boldsymbol{\varphi}(\mathbf{e}_0; T_c, m). \quad (10)$$

Then, according to the equation (4), (5), (9) and (10), the joint angular velocity trajectory of the FFSR with predefined-time convergence can be deduced:

$$\dot{\boldsymbol{\Theta}}^1 = (\mathbf{J}_m^1)^{-1} (\mathbf{J}_e^{-1} (\mathbf{J}_{ed} \mathbf{V}_{ed} - \boldsymbol{\varphi}(\mathbf{e}_1; T_c, m)) - \mathbf{J}_0 \mathbf{V}_0), \quad (11)$$

$$\dot{\boldsymbol{\Theta}}^2 = (\mathbf{J}_c^2)^{-1} (\mathbf{J}_c^1 \dot{\boldsymbol{\Theta}}^1 - \boldsymbol{\varphi}(\mathbf{e}_0; T_c, m) \mathbf{J}_b^{-1} \mathbf{H}_0 - \mathbf{C}). \quad (12)$$

If \mathbf{J}_m^1 or \mathbf{J}_c^2 is a singular matrix, a DLS algorithm in [13] can be adopted in the trajectory planning of the FFSR to obtain a non-singular joint angular velocity trajectory $\dot{\boldsymbol{\Theta}}^j$, then, the equations (11) and (12) can be expressed as:

$$\dot{\boldsymbol{\Theta}}^1 = \text{diag}(\sum_{i=1}^6 \frac{\sigma_i^1}{\sigma_i^1 + (\lambda_i^1)^2} v_i^1 (u_i^1)^T) (\mathbf{J}_e^{-1} (\mathbf{J}_{ed} \mathbf{V}_{ed} - \boldsymbol{\varphi}(\mathbf{e}_1; T_c, m)) - \mathbf{J}_0 \mathbf{V}_0) \quad (13)$$

$$\dot{\boldsymbol{\Theta}}^2 = \text{diag}(\sum_{i=1}^6 \frac{\sigma_i^2}{\sigma_i^2 + (\lambda_i^2)^2} v_i^2 (u_i^2)^T) (\mathbf{J}_c^1 \dot{\boldsymbol{\Theta}}^1 - \boldsymbol{\varphi}(\mathbf{e}_0; T_c, m) \mathbf{J}_b^{-1} \mathbf{H}_0 - \mathbf{C}). \quad (14)$$

where $\text{diag}(A_i) = \begin{bmatrix} A_1 & \cdots & 0 \\ \vdots & \ddots & \vdots \\ 0 & \cdots & A_6 \end{bmatrix}$, in which $i = 1, 2, \dots, 6$. Here, λ_i^j can be expressed as:

$$\lambda_i^j = \begin{cases} \lambda_m \left(1 + \frac{|\sigma_i^j|}{\varepsilon^j} \right), & |\sigma_i^j| \leq \varepsilon^j \\ 0, & |\sigma_i^j| > \varepsilon^j \end{cases} \quad (15)$$

in which λ_m is a damping factor, ε^j is the singular threshold value.

Obstacle-avoidance Trajectory Planning for a Dual-arm FFSR

In space, the floating satellite debris and micrometeorites may pose a collision risk to the robotic arm. Hence, a CDF-based trajectory planning method in [14] will be adopted to enable the space robot to avoid the collision.

$$\begin{aligned} \dot{\Theta}^1 = & \mu \cdot (\mathbf{J}_m^1)^T \cdot \text{diag} \left(\sum_{i=1}^6 \frac{\sigma_i^1}{\sigma_i^1 + (\lambda_i^1)^2} v_i^1 (u_i^1)^T \right) (\mathbf{J}_e^{-1} (\mathbf{J}_{ed} \mathbf{V}_{ed} - \mathbf{k} \mathbf{e}_1) \\ & - \mathbf{J}_0 \mathbf{V}_0) + [\mathbf{E} - \mu (\mathbf{J}_m^1)^T (\mathbf{J}_m^1 (\mathbf{J}_m^1)^T)^{-1} \mathbf{J}_m^1] \dot{\Theta}_c^1 \end{aligned} \quad (16)$$

$$\begin{aligned} \dot{\Theta}^2 = & \mu \cdot (\mathbf{J}_c^2)^T \cdot \text{diag} \left(\sum_{i=1}^6 \frac{\sigma_i^2}{\sigma_i^2 + (\lambda_i^2)^2} v_i^2 (u_i^2)^T \right) (\mathbf{J}_c^1 \dot{\Theta}^1 - \mathbf{k} \cdot \mathbf{J}_b^{-1} \mathbf{H}_0 \mathbf{e}_0 - \mathbf{C}) \\ & + [\mathbf{E} - \mu (\mathbf{J}_c^2)^T (\mathbf{J}_c^2 (\mathbf{J}_c^2)^T)^{-1} \mathbf{J}_c^2] \dot{\Theta}_c^2 \end{aligned} \quad (17)$$

where $\dot{\Theta}_c^j$ is the overall collision-avoidance joint angular velocity of Arm-j; the weighted coefficient μ can be expressed as :

$$\mu = \begin{cases} 0, & \text{if } L_p \geq (1 + \xi)\Delta \\ \frac{|L_p - (1 + \xi)\Delta|}{2\xi\Delta}, & \text{otherwise} \\ 1, & \text{if } L_p \leq (1 - \xi)\Delta \end{cases} \quad (18)$$

in which $L_p = \max\|\mathbf{CDF}(\mathbf{p})\|$ and \mathbf{CDF} is a risk function of the collision field between the robotic arm and obstacle; $\xi < 1$ is a constant and Δ is the threshold value of collision.

However, the traditional low-error CDF-based trajectory planning method is based on the proportional feedback [14], but it cannot deal well with the timing tasks and large danger filed. Therefore, similar to (13) and (14), a predefined-time stability is also applied in the pose-feedback-based-kinematic equations (16) and (17) to get the following collision-avoidance joint angular velocity trajectory of Arm-j ($j=1,2$):

$$\begin{aligned} \dot{\Theta}^1 = & \mu \cdot (\mathbf{J}_m^1)^T \cdot \text{diag} \left(\sum_{i=1}^6 \frac{\sigma_i^1}{\sigma_i^1 + (\lambda_i^1)^2} v_i^1 (u_i^1)^T \right) (\mathbf{J}_e^{-1} (\mathbf{J}_{ed} \mathbf{V}_{ed} - \boldsymbol{\varphi}(\mathbf{e}_1; T_c, m)) \\ & - \mathbf{J}_0 \mathbf{V}_0) + [\mathbf{E} - \mu (\mathbf{J}_m^1)^T (\mathbf{J}_m^1 (\mathbf{J}_m^1)^T)^{-1} \mathbf{J}_m^1] \dot{\Theta}_c^1 \end{aligned} \quad (19)$$

$$\begin{aligned} \dot{\Theta}^2 = & \mu \cdot (J_c^2)^T \cdot \text{diag} \left(\sum_{i=1}^6 \frac{\sigma_i^2}{\sigma_i^2 + (\lambda_i^2)^2} v_i^2 (u_i^2)^T \right) (J_c^1 \dot{\Theta}^1 - \varphi(e_0; T_c, m) J_b^{-1} H_0 - C) \\ & + [E - \mu (J_c^2)^T (J_c^2 (J_c^2)^T)^{-1} J_c^2] \dot{\Theta}_c^2 \end{aligned} \quad (20)$$

GA-based Optimal Trajectory Planning for a Dual-arm FFSR

Even if we adopt obstacle-avoidance and singularity-avoidance strategies in trajectory planning for the space robot, there is still a big problem that restricts the mission success of capture, which is the over-saturation of the robotic joint angular velocity. The maximum joint angular velocity of the mechanical system has to be controlled within a limited range, and its durability will be seriously affected if the robotic arm stays at a large joint angular velocity for a long time. Even the gear may be twisted to break in that case. Hence, an optimization of joint angular velocity should be adopted in the dual-arm FFSR system to get a smaller and smoother joint angular velocity of robotic arm. In this study, a GA-based optimal strategy is adopted in trajectory planning process, and the objective function \mathbf{B} can be established as the following:

$$\mathbf{B} = \gamma(\alpha \int \Psi(\|\dot{\Theta}^1\|, \dot{\Theta}_{danger}^1) + \beta \int \Psi(\|\dot{\Theta}^2\|, \dot{\Theta}_{danger}^2)) + \Theta_b \quad (21)$$

where α , β and γ are the weight parameters, $\dot{\Theta}_{danger}^j$ represents the an estimate that the joint angular velocity of Arm-j is approaching saturation. if $A > B$, $A = \Psi(A, B)$, else $0 = \Psi(A, B)$. The limiting factor of joint angular velocity Θ_b can be given as:

$$\Theta_b = \begin{cases} +\infty & , & \dot{\Theta}^2 > \dot{\Theta}_{+max} \\ +\infty & , & \dot{\Theta}^2 < \dot{\Theta}_{-max} \\ 0 & , & \dot{\Theta}_{-max} < \dot{\Theta}^2 < \dot{\Theta}_{+max} \end{cases} \quad (22)$$

in which $\dot{\Theta}_{\pm max}$ is the value of over-saturation of joint angular velocity $\dot{\Theta}^j$.

The genetic optimal algorithm can be described as:

Step a (the initialization of genetic population):

The population is composed by the two-dimensional array of predefined-time parameter m and T_c , and the size of population can be denoted by S_{max} . Then, S_{max} joint angular velocity trajectories of dual-arm will generate to form the initial population. In the end, the joint angular velocity trajectories in initial population will be substituted into the fitness function, which is just the objection function \mathbf{B} , to obtain the initial best individual fitness.

Step b (evaluation):

The purpose of evolution is to imitate the genetic inheritance of the biological population in nature and get a new generation by selecting mating, crossing and genetic variation. The fitness function is then used to select the best individual of the next generation.

Step c (selection):

The selection of this GA algorithm is roulette selection strategy. The probability of fitness can be expressed as:

$$P_{st} = \frac{B(x_i)}{\sum_{i=1}^{S_{max}} B(x_i)} \quad (23)$$

where \mathbf{x}_i is the i -th individual, and $\mathbf{x} = [\boldsymbol{\theta}^1 \quad \boldsymbol{\theta}^2]$. It is clear that the individual of will high fitness probability will be selected more times, because the gambling ball will be more likely to swing into a larger roulette area.

Step d (cross):

After selection, two individual are selected to cross by the crossing probability P_c , but the cross-point of individuals are chosen randomly.

Step e (mutation):

After cross, two individual are selected to mutate by the mutating probability P_m , but the cross-point of individuals are chosen randomly.

Step f (new population):

After first generation of evaluation, we will continue to evolve in G generations until the curves for average fitness and best fitness converge.

Simulation

The proposed space robotic arm is PUMA-560 type, and its D-H structure is shown in the Fig. 2. The parameters of D-H and machine have been reset to Table I and Table II. The simulation is based on MATLAB2016b, the simulating step is ode45.

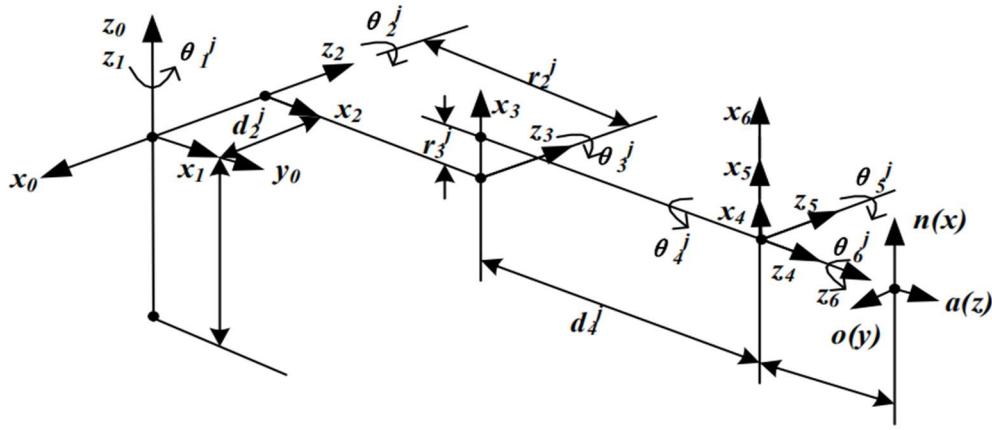


Figure 2. The D-H frame of Arm-j

Table I. The D-H parameters of PUMA560-type Robotic Arm-j.

Joint ^j	$\theta_i^j(\text{m})$	$d_{i-1}^j(\text{m})$	$r_{i-1}^j(\text{m})$	$A_i^j(^{\circ})$
1	θ_1	0	0	0
2	θ_2	0	0	-90
3	θ_3	0	0.6	0
4	θ_4	0.4	0.6	-90
5	θ_5	0	0	90
6	θ_6	0	0	-90

Table II. Table II. The math properties of Arm-j.

	Base	Link 1	Link 2	Link 3	Link 4	Link 5	Link 6
Mass(kg)	400	6	4	4	4	3	2
$a_{ix}^j(\text{m})$	\	0	0.20	0.20	0	0	0
$a_{iy}^j(\text{m})$	\	0	0	0.20	0	0	0

$a_{iz}^j(\text{m})$	\	0	0.20	0	0	0	0
$b_{ix}^j(\text{m})$	-0.36	0	0.20	0.20	0	0	0
$b_{iy}^j(\text{m})$	0	0	0	0.20	0	0	0
$b_{iz}^j(\text{m})$	-0.42	0	0.20	0	0	0	0
$I_{xx}^j(\text{kg}\cdot\text{m}^2)$	30	0.15	0.09	0.11	1.05	1.03	1.02
$I_{yy}^j(\text{kg}\cdot\text{m}^2)$	28	0.15	0.91	0.11	1.05	1.03	1.02
$I_{zz}^j(\text{kg}\cdot\text{m}^2)$	32	0.08	0.85	0.03	1.05	1.03	1.02
$I_{xy}^j(\text{kg}\cdot\text{m}^2)$	0.26	0	0	0	0	0	0
$I_{xz}^j(\text{kg}\cdot\text{m}^2)$	0.37	0	0	0	0	0	0
$I_{yz}^j(\text{kg}\cdot\text{m}^2)$	-0.29	0	0	0	0	0	0

The initial momentum of the FFSR system \mathbf{C} are set to 0, the simulation time is 20s. The initial position and attitude of base are $\mathbf{p}_{b0} = [-0.2832 \ 0.3107 \ 0.3248]^T(\text{m})$ and $\boldsymbol{\sigma}_{b0} = [1 \ 0 \ 0 \ 0]^T$, respectively. The initial position and attitude of end-effector can be set to: $\mathbf{p}_{e0} = [-0.2832 \ 0.3107 \ 0.3248]^T(\text{m})$ and $\boldsymbol{\sigma}_{e0} = [0 \ 0.8191 \ 0 \ 0.5736]^T$, respectively.

The initial joint angle of Arm-j are $\boldsymbol{\Theta}_0^1 = [0 \ 47.72 \ -93.91 \ 0 \ -23.82 \ 0]^T(\circ)$ and $\boldsymbol{\Theta}_0^2 = [0 \ -47.72 \ 176.09 \ 0 \ -23.82 \ 0]^T(\circ)$, respectively.

The position and attitude of the target are: $\mathbf{p}_t = [0.7147 \ 0.4150 \ -0.1758]^T(\text{m})$ and $\boldsymbol{\sigma}_t = [0.0215 \ 0.9027 \ 0.1184 \ 0.4132]^T$, respectively. The position of the obstacle point is $\mathbf{p}_o = [-0.0691 \ 0.6037 \ 0.4742]^T(\text{m})$, and the danger radius is set to 0.2 (m).

The initial parameter of singularity-avoidance algorithm can be set to:

$$\lambda_m = 0.08, \varepsilon^j = 0.02.$$

As shown in the Figure 3, a velocity-level path planning of end-effector is adopted to get a desired trapezoidal velocity trajectory of end-effector.

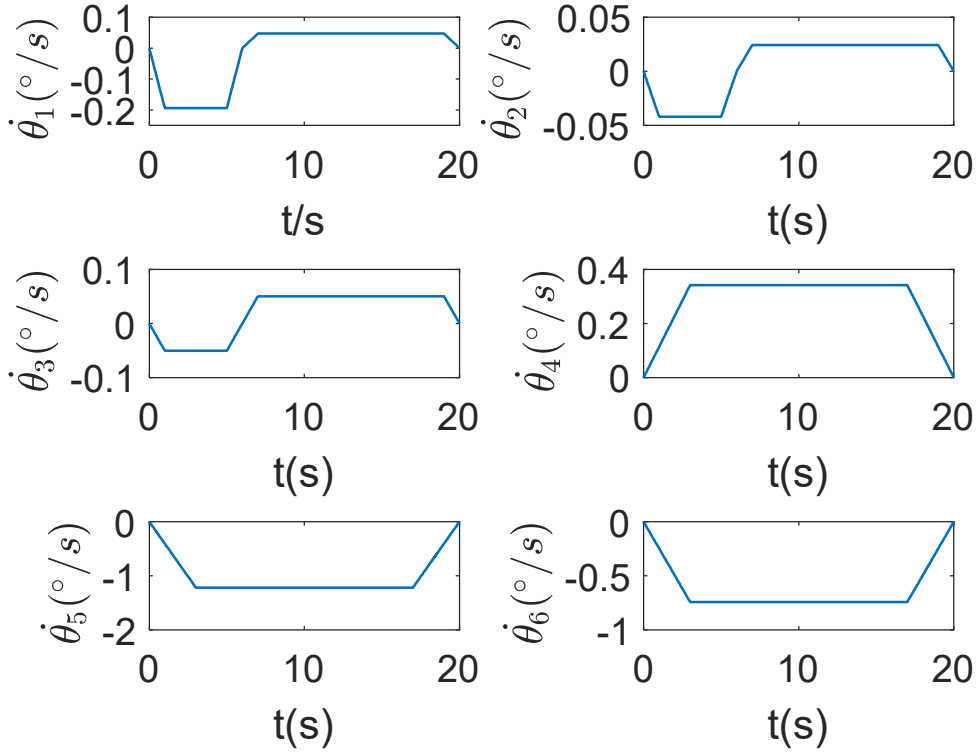


Figure 3. The desired trapezoidal velocity-level trajectory of end-effector

An optimal obstacle-avoidance trajectory planning method will be discussed in this simulation. The precision of the method should be high enough to improve the success rate of space-capture mission, and the time to return stability after avoiding obstacles should be predictable. Furthermore, similar to the finite time controller, the exponential convergence based pose feedback will also increase the joint angular velocity equivalent to control input. Therefore, we should optimize the parameters to achieve the minimum joint angular velocity trajectory.

Pose-feedback-based Trajectory Planning for a Dual-arm FFSR with Predefined-time Convergence

Different from singularity-avoidance algorithm [13], the accumulated error caused by obstacle avoidance is far greater than the instantaneous singularity, so the proportional-convergence-based pose feedback may not make this error converge to the micro-scale neighbourhood of zero, (or the convergence time is so long that the error cannot be eliminated). In order to compare the tracking accuracy of the proposed algorithm with the previous one, a trajectory planning method without obstacle-avoidance (no obstacle-avoidance algorithm), a no-pose-feedback obstacle-avoidance algorithm [20] (no pose feedback) and a CDF-based trajectory planning method with proportional-convergence-based pose feedback [14] (the proportional pose feedback) will be simulated to compare with the proposed method. The parameters of CDF-based obstacle-avoidance algorithm are set to: $\xi = 0.1$ and $\Delta = 17.25$. The predefined-time parameters are set to: $m = 0.1$ and $T_c = 3$.

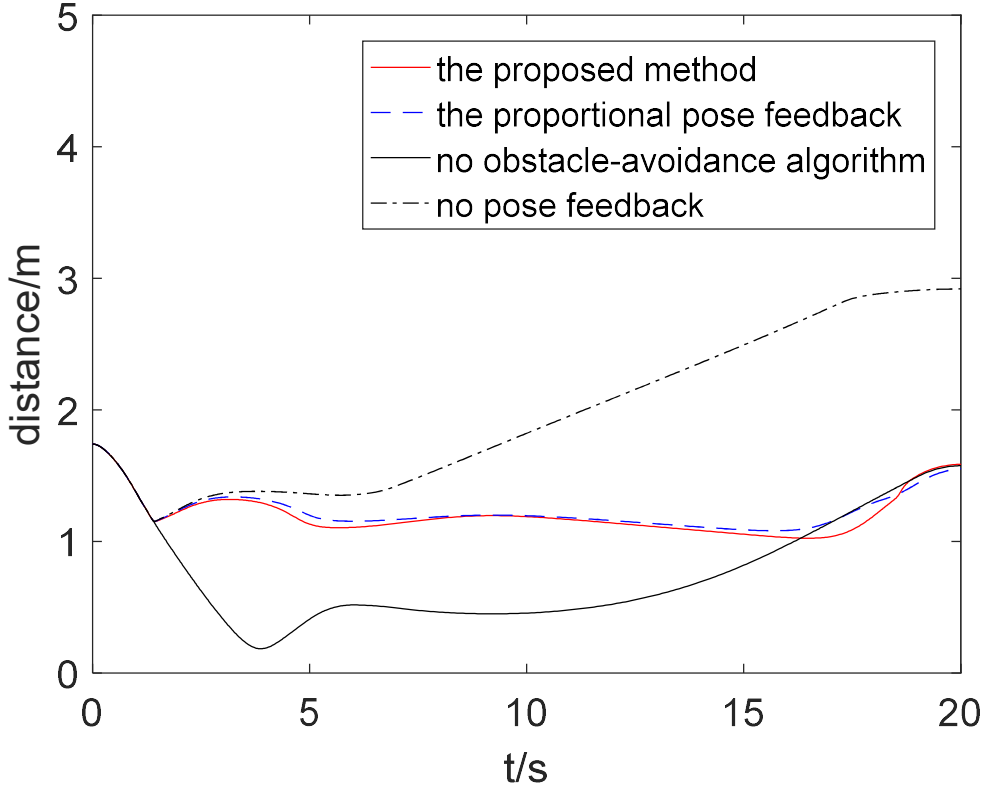


Figure 4. The curve of the closest distance between the obstacle point and the arm

As shown in the Figs. 4, the proposed method and other CDF-based trajectory planning method can keep the robotic arm from hitting the obstacle point, and the trajectory planning method without obstacle-avoidance algorithm will crash the robotic arm into an obstacle. According to the Fig. 5, it is clear that the proposed method and proportional pose-feedback-based method can make error converge to a small neighbourhood of zero, but the position error of end-effector in a trajectory planning method without obstacle-avoidance can only exist forever. Compared the proportional pose-feedback-based method with the proposed method, by Fig. 5, it is clear that the accumulated error caused by obstacle avoidance will be difficult to eliminate through proportional feedback, but exponential feedback is doing better. The final error of end-effector in proportional feedback is 0.033m, and the final error of end-effector in exponential feedback is 8.922×10^{-12} m. Therefore, a predefined-time stability system should be applied in trajectory planning to enable the pose errors of end-effector to converge within a predetermined time T_c . The actual convergence time of position error of end-effector is only 1.198s, which is less than the estimated time $T_c = 3$ s. Furthermore, as shown in the Fig 6, the attitude error of end-effector and the pose error of base can also be converged to the micron-scale neighbourhood of zero by the proposed algorithm, and the convergence time is also less than $T_c = 3$ s.

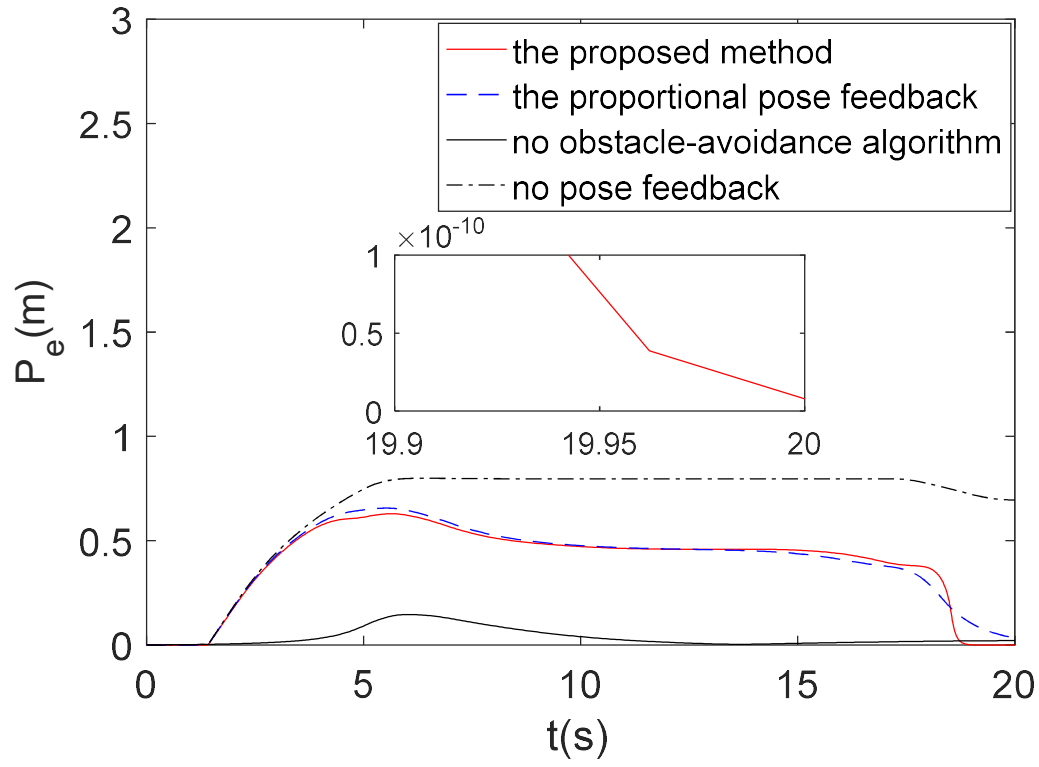
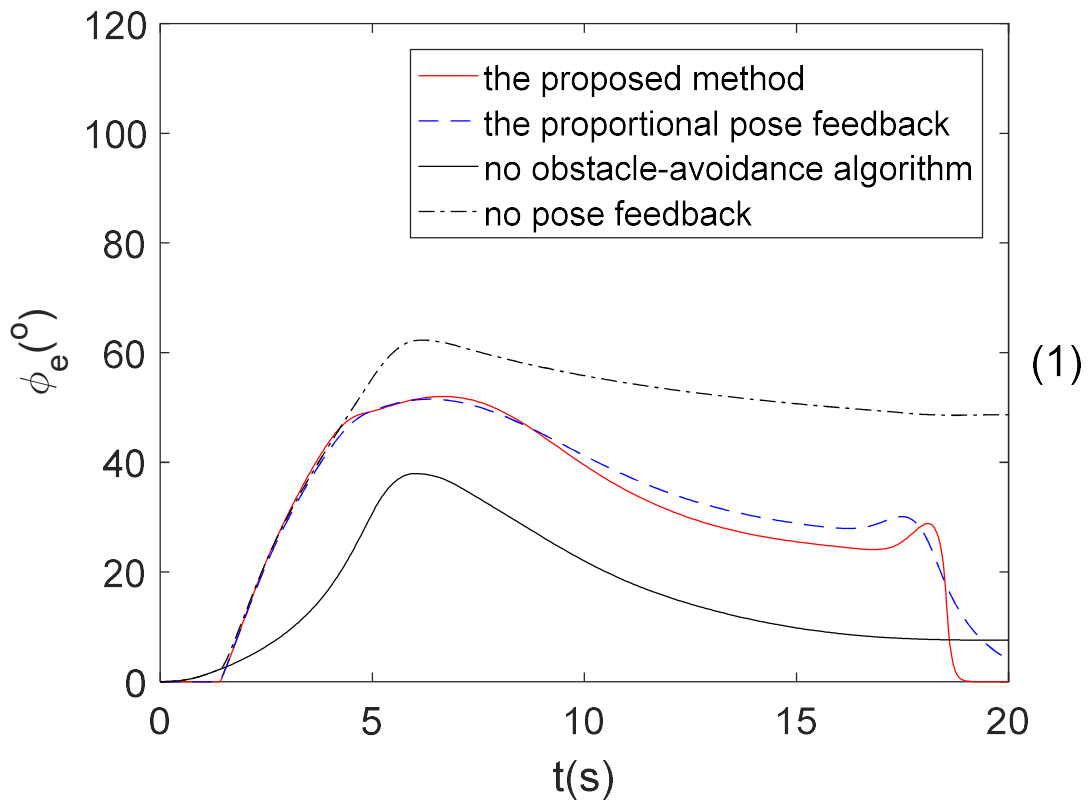


Figure 5. The position error curve of the end-effector (three axis synthesis)



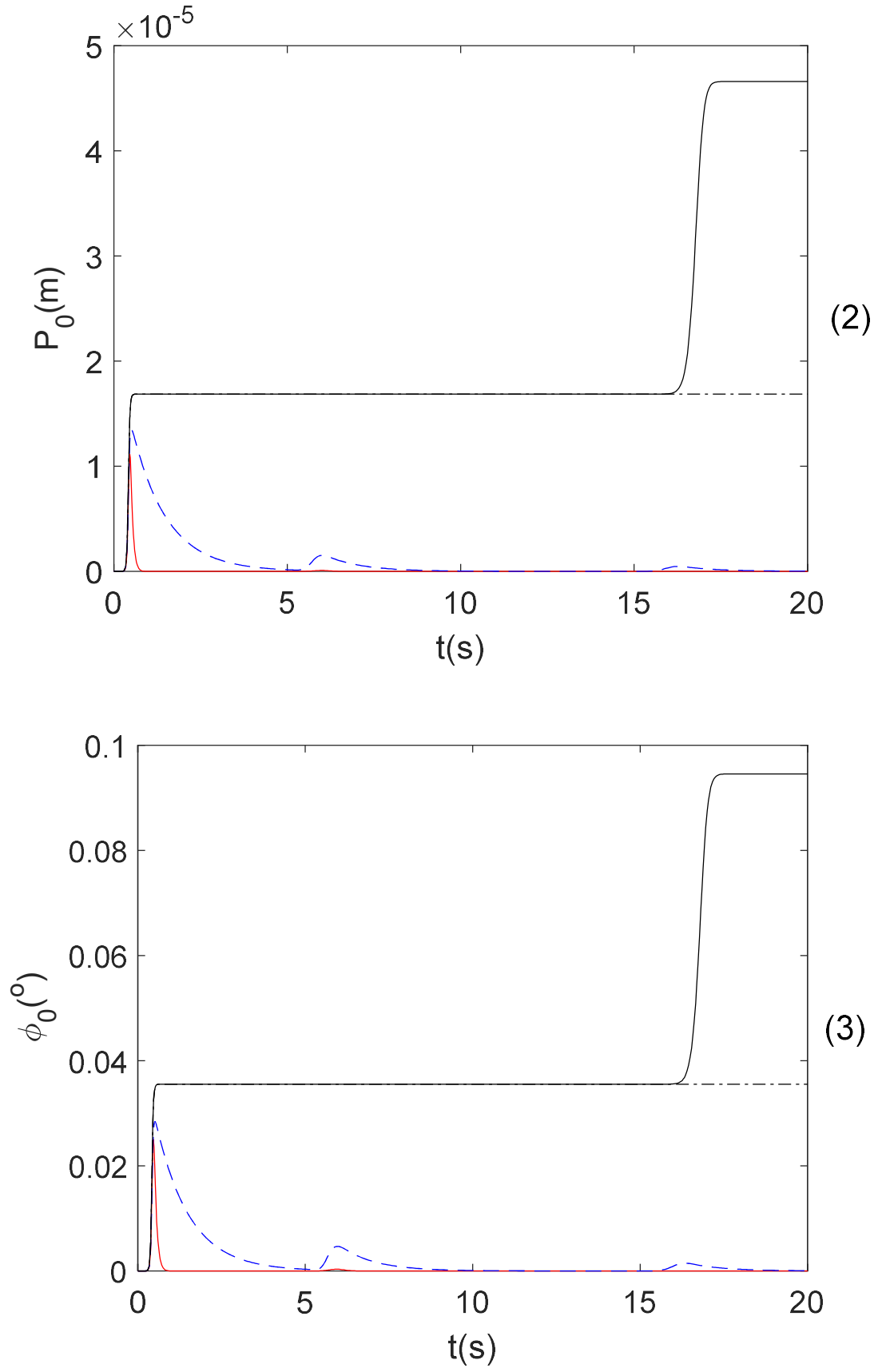


Figure 6. (1) The attitude error curve of the end-effector; (2) The position error curve of the base (three axis synthesis); (3) The position error curve of the base

GA-based Optimal Micron-scale Predefined-time Trajectory Planning for a Dual-arm FFSR

Based on the above predefined-time trajectory planning method, we study a GA-based parameter optimization strategy. Similar to all finite-time feedback control, the terminal attractor in the exponential term will cause the initial control input, which is just the angular velocity of robotic arm, to become very large. Hence, in order to improve the durability of the manipulator, we need to optimize the parameters to get the best angular velocity trajectory of the joint.

The initial parameters of genetic algorithm can be set to:

$$\alpha = 0.35, \beta = 0.65, \gamma = 0.0001, \dot{\theta}_{danger}^j = 150^\circ/s \text{ and } \dot{\theta}_{\pm max} = \pm 200^\circ/s, \\ S_{max} = 100, P_c = 0.6, P_m = 0.1, G=100.$$

The predefined-time parameter in no GA method can be set to:

$$m = 0.1, T_c = 2.19.$$

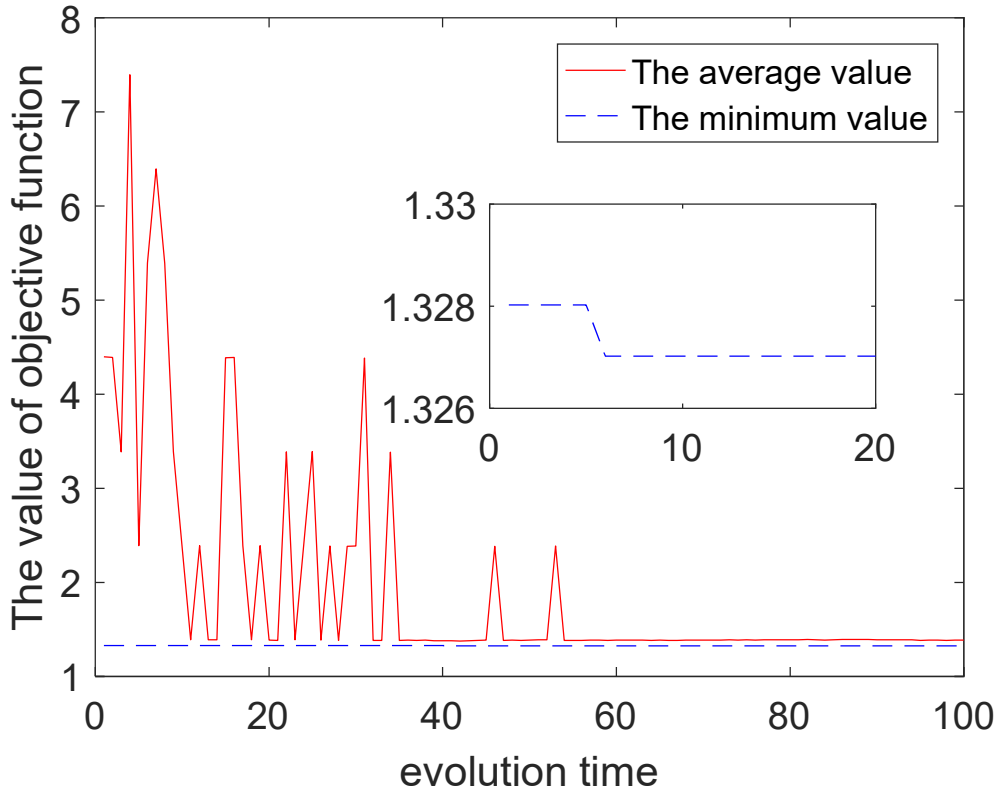


Figure 7. The each generation value of GA

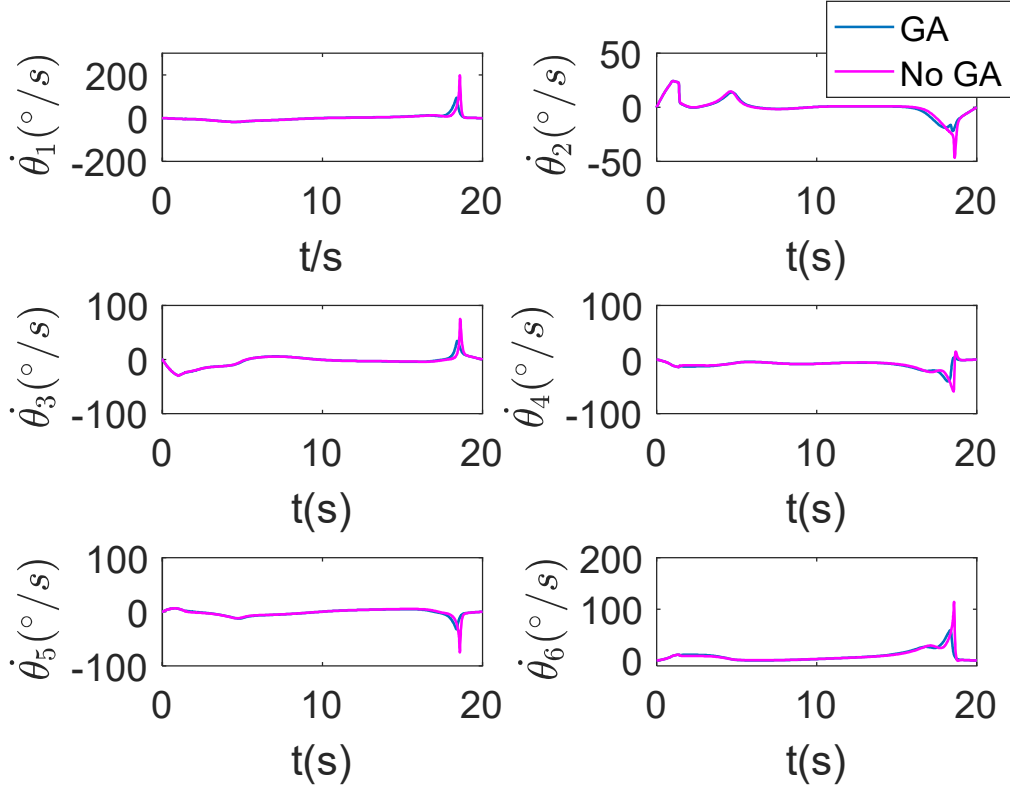


Figure 8. The joint angular velocity of mission arm

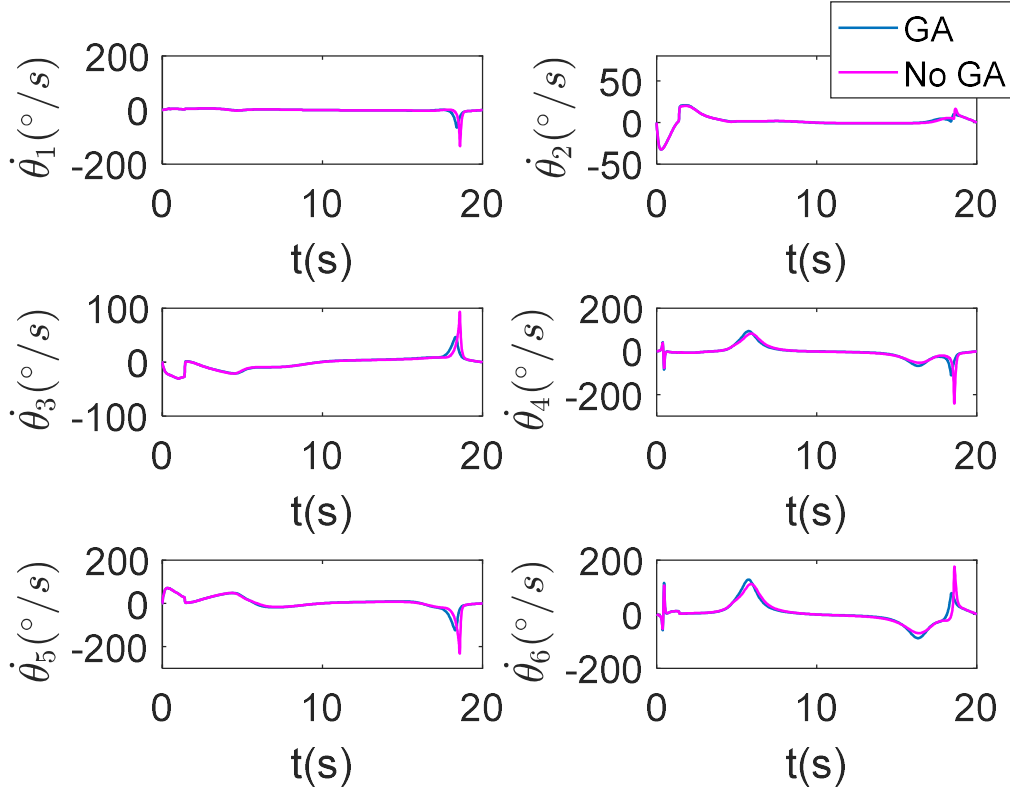


Figure 9. The joint angular velocity of balance arm

The comparison methods are the proposed GA-based algorithm and the predefined-time trajectory planning without optimal algorithm (for fair, the predefined-time function forms and time parameters T_c of the comparison methods are consistent). According to the result in

Fig. 7, the optimal predefined-time parameter can be set to $m = 0.2167$, $T_c = 2.19$. As shown in the Fig. 8 and 9, it is clear that the joint angular velocity in GA-based predefined-time trajectory planning method is smoother and smaller than the same method without optimal algorithm in whole. The max joint angular velocity of mission arm in GA-based method is $\theta_1^1 = 94.12^\circ/\text{s}$, but the non-optimal method is $\theta_1^1 = 198.40^\circ/\text{s}$. The max joint angular velocity of balance arm in GA-based method are $\theta_4^2 = -110.70^\circ/\text{s}$ and $\theta_5^2 = -124.00^\circ/\text{s}$, but the non-optimal method are $\theta_4^2 = -241.40^\circ/\text{s}$ and $\theta_5^2 = -231.90^\circ/\text{s}$. Furthermore, according to the Fig. 10, the micron-level pose tracking precision of end-effector can also be guaranteed. The final error of end-effector in exponential feedback is just $2.816 \times 10^{-7}\text{m}$, and the convergence time is 1.751s, which is less than the predefined time $T_c = 2.19\text{s}$.

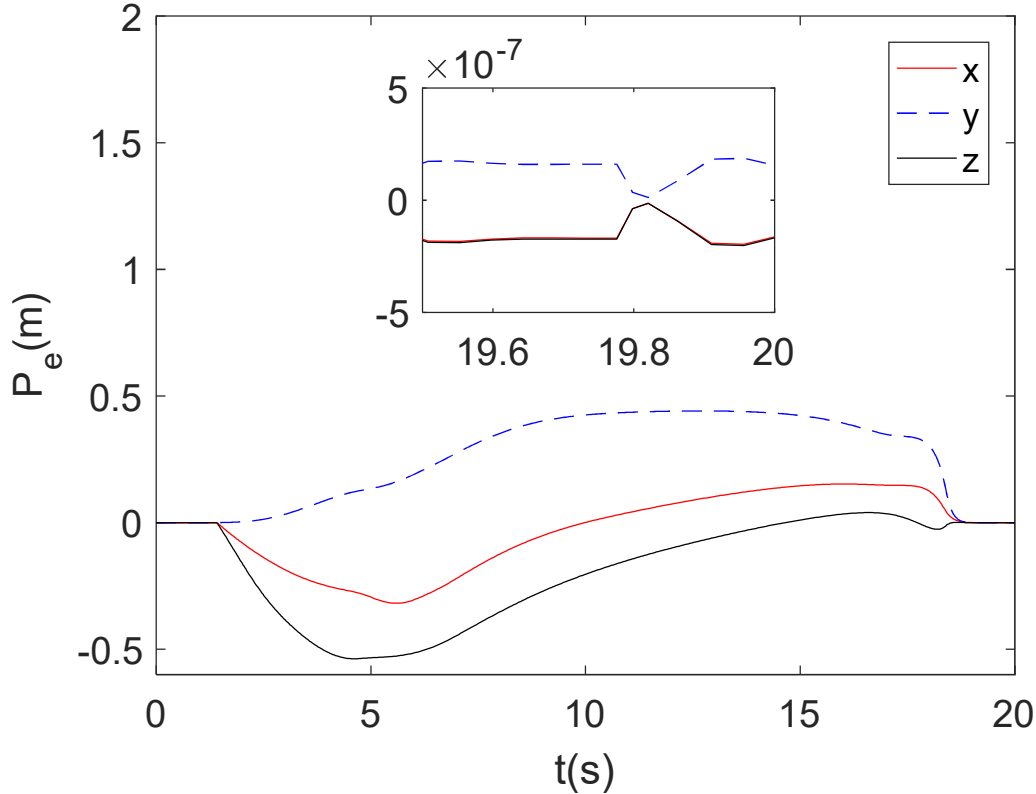


Figure 10. The position error curve of the end-effector in the proposed method with GA

Conclusions

This paper addresses the optimization in predefined-time obstacle-avoidance trajectory planning for a space robot. In our previous study [13], the joint angular velocity trajectory planning of robotic arm was used to control the convergence rate of the pose tracking error of end-effector. However, if we apply exponential feedback in the pose-based kinematic equation to obtain an error rapid response form, the joint angular velocity of robotic arm, especially the balance arm, will become too large to damage the mechanism drive system. Hence, a GA-based optimal strategy should be adopted in trajectory planning for the space robot to obtain a small and smooth joint angular velocity trajectory. This work is different from the traditional optimization strategy of manipulator trajectory planning. We no longer consider the tracking error and smoothness of trajectory at the same time, but apply the predefined-time pose feedback to obtain the theoretical zero-error tracking precision so that only the smoothness of trajectory is considered. In the future, we will explore the machine-vision-based optimal trajectory tracking control for a space robot with a predefined-time-convergent neural network.

Appendix

The velocity-level kinematic of the robotic end-effector can be expressed as:

$$\mathbf{V}_e = \mathbf{J}_0 \mathbf{V}_0 + \mathbf{J}_m^1 \dot{\boldsymbol{\theta}}^1, \quad (24)$$

$$\begin{cases} \mathbf{P} = \mathbf{M}[\mathbf{E} & -\tilde{\mathbf{r}}_{0g}] \begin{bmatrix} \mathbf{V}_0 \\ \mathbf{w}_0 \end{bmatrix} + \mathbf{J}_{Tw}^1 \dot{\boldsymbol{\theta}}^1 + \mathbf{J}_{Tw}^2 \dot{\boldsymbol{\theta}}^2 \\ \mathbf{L} = [\mathbf{M}\tilde{\mathbf{r}}_g & \mathbf{E}] \begin{bmatrix} \mathbf{V}_0 \\ \mathbf{w}_0 \end{bmatrix} + \mathbf{H}_{w\phi}^1 \dot{\boldsymbol{\theta}}^1 + \mathbf{H}_{w\phi}^2 \dot{\boldsymbol{\theta}}^2 \end{cases}. \quad (25)$$

where $[\mathbf{P} \ \mathbf{L}]^T = \mathbf{C}$ is the linear and angular momentum matrix of the FFSR system, respectively. \mathbf{M} is the total mass of the FFSR system. $\tilde{\mathbf{r}}_g$ is the cross-product position vector of system centroid and $\tilde{\mathbf{r}}_{0g}$ is the cross-product position vector from the system centroid to base. \mathbf{J}_{Tw}^j and $\mathbf{H}_{w\phi}^j$ can be written as:

$$\mathbf{J}_c^1 = [\mathbf{J}_{Tw}^1 \ \mathbf{H}_{w\phi}^1]^T, \quad \mathbf{J}_c^2 = [\mathbf{J}_{Tw}^2 \ \mathbf{H}_{w\phi}^2]^T. \quad (26)$$

Then, the velocity-level kinematic of the satellite base can be expressed as:

$$\mathbf{V}_0 = \mathbf{C} - \mathbf{J}_c^1 \dot{\boldsymbol{\theta}}^1 - \mathbf{J}_c^2 \dot{\boldsymbol{\theta}}^2. \quad (27)$$

The pose errors of the end-effector and base can be defined as:

$$\begin{cases} \mathbf{e}_e = \mathbf{p}_e - \mathbf{p}_{ed} \\ \mathbf{q}_e = \mathbf{q}_{ed}^{-1} \mathbf{q}_{ee} \end{cases}, \quad \begin{cases} \mathbf{e}_0 = \mathbf{p}_0 - \mathbf{p}_{0d} \\ \mathbf{q}_0 = \mathbf{q}_{0d}^{-1} \mathbf{q}_{00} \end{cases}. \quad (28)$$

where \mathbf{p}_e , \mathbf{p}_{ed} , \mathbf{p}_0 and \mathbf{p}_{0d} are the actual and desired position of the robotic end-effector, respectively. $\mathbf{q}_e^T = [q_{e0} \ q_{e1} \ q_{e2} \ q_{e3}] = [q_{e0} \ \mathbf{q}_{ev}]$ is the attitude quaternion of error of manipulator. \mathbf{q}_{ee} and \mathbf{q}_{ed} are the actual and desired attitude quaternion of error of the robotic end-effector, respectively. Similarly, $\mathbf{q}_0^T = [q_{00} \ q_{01} \ q_{02} \ q_{03}] = [q_{00} \ \mathbf{q}_{0v}]$. \mathbf{q}_{00} and \mathbf{q}_{0d} are the actual and desired attitude quaternion of error of the satellite base, respectively.

The attitude errors of the end-effector and base can be expressed by MRP:

$$\boldsymbol{\sigma}_e = \frac{\mathbf{q}_{ev}}{1+q_{e0}}, \quad \boldsymbol{\sigma}_0 = \frac{\mathbf{q}_{0v}}{1+q_{00}} \quad (29)$$

In the end, the pose-error kinematic relationship of the robotic end-effector and base can be deduced by the above-mentioned equations (24), (27), (28) and (29).

Conflicts of Interest

The authors declare that there is no conflict of interest regarding the publication of this paper.

Funding Statement

This work was supported by Major Special Project of the Science and Technology on Intelligent Manufacturing and Robot under Grant 2019ZDZX0019.

References

- [1] T. Fong, M. Bualat, L. Edwards, “Human-robot site survey and sampling for space exploration,” in *Space 2006*, pp. 7425, San Jose, California, September 2006.
- [2] W. Xu, B. Liang, and Y. Xu, “Survey of modeling, planning, and ground verification of space robotic systems,” *Acta Astronautica*, vol. 68, no. 11–12, pp. 1629–1649, 2011.
- [3] A. Flores-Abad, O. Ma, K. Pham, and S. Ulrich, “A review of space robotics technologies for on-orbit servicing,” *Progress in Aerospace Sciences*, vol. 68, pp. 1–26, 2014.
- [4] J. Liu, Y. Shi, Z. M. Fadlullah, and N. Kato, “Space-air-ground integrated network: A survey,” *IEEE Communications Surveys & Tutorials*, vol. 20, no. 4, pp. 2714–2741, 2018.
- [5] S. Nishida, S. Kawamoto, Y. Okawa, F. Terui, and S. Kitamura, “Space debris removal system using a small satellite,” *Acta Astronautica*, vol. 65, no. 1–2, pp. 95–102, 2009.
- [6] H. Klinkrad, “Space debris,” *Encyclopedia of Aerospace Engineering*, vol. 2010, 2010.
- [7] S. Nishida, and T. Yoshikawa, “Capture and motion braking of space debris by a space robot,” in *2007 International Conference on Control, Automation and Systems*, pp. 706–711, Seoul, South Korea, October 2007.
- [8] P. Huang, F. Zhang, J. Cai, D. Wang, Z. Meng, and J. Guo, “Dexterous tethered space robot: Design, measurement, control, and experiment,” *IEEE Transactions on Aerospace and Electronic Systems*, vol. 53, no. 3, pp. 1452–1468, 2017.
- [9] Y. Xu, “The measure of dynamic coupling of space robot systems,” in *[1993] Proceedings IEEE International Conference on Robotics and Automation*, pp. 615–620, Atlanta, GA, USA, USA, May 1993.
- [10] S. K. Agrawal, and S. Shirumalla, “Planning motions of a dual-arm free-floating manipulator keeping the base inertially fixed,” *Mechanism and Machine Theory*, vol. 30, no. 1, pp. 59–70, 1995.
- [11] H. Zhao, C. Wang, and Z. Guo, “Coordinated dynamics control of a free-floating dual-arm space robot,” *Modern Applied Science*, vol. 4, no. 5, pp. 175, 2010.
- [12] L. Yan, Z. Mu, and W. Xu, “Base centroid virtual manipulator modeling and applications for multi-arm space robots,” in *2014 13th International Conference on Control Automation Robotics & Vision (ICARCV)*, pp. 1542–1547, Singapore, Singapore, December 2014.
- [13] Y. Liu, K. Xie, T. Zhang, and N. Cai, “Trajectory planning with pose feedback for a dual-arm space robot,” *Journal of Control Science and Engineering*, vol. 2016, 2016.
- [14] Y. Liu, C. Yu, J. Sheng, and T. Zhang, “Self-collision avoidance trajectory planning and robust control of a dual-arm space robot,” *International Journal of Control, Automation and Systems*, vol. 16, no. 6, pp. 2896–2905, 2018.

- [15] Y. Yokose, “Trajectory planning for a manipulator with nonlinear Coulomb friction using a dynamically incremental genetic algorithm,” *Artificial Life and Robotics*, vol. 22, no. 1, pp. 31–35, 2017.
- [16] W. Chen, H. Fang, Y. Yang, and W. He, “Optimal Trajectory Planning for Delta Robot Based on Three-parameter Lamé Curve,” In *2017 2nd International Conference on Cybernetics, Robotics and Control (CRC)*, pp. 39–44, Chengdu, China, July 2017.
- [17] J. Wu, D. Bin, X. Feng, Z. Wen, and Y. Zhang, “GA based adaptive singularity-robust path planning of space robot for on-orbit detection,” *Complexity*, vol. 2018, 2018.
- [18] J. D. Sánchez-Torres, E. N. Sanchez, and A. G. Loukianov, “Predefined-time stability of dynamical systems with sliding modes,” In *2015 American control conference (ACC)*, pp. 5842–5846, Chicago, IL, USA, July 2015.
- [19] M. Idan, “Estimation of Rodrigues parameters from vector observations,” *IEEE Transactions on Aerospace and Electronic Systems*, vol. 32, no. 2, pp. 578–586, 1996.
- [20] B. Lacevic, P. Rocco, and A. M. Zanchettin, “Safety assessment and control of robotic manipulators using danger field,” *IEEE Transactions on Robotics*, vol. 29, no. 5, pp. 1257–1270, 2013.